Clear Aperture Design Criterion for Deformable Membrane Mirror Control

Michael J. Shepherd
Richard G. Cobb
Department of Aeronautics and Astronautics

William P. Baker
Department of Mathematics and Statistics

Air Force Institute of Technology
2950 Hobson Way
Wright Patterson AFB, OH 45433-7765, USA
937-255-3636 ext 4559
richard.cobb@afit.edu

Abstract— **Active lightweight continuous mirrors, such as deformable membrane mirrors, provide the capability to form conjugate surfaces effective for removing atmospheric distortions of an incoming wavefront. For a circular aperture, the two-dimensional surface corrections are most often described by a truncated set of the Zernike polynomial basis functions. Simultaneously, there exists a requirement in active lightweight membrane mirrors to resist the effects of vibration disturbances which could build at resonance and adversely distort the membrane surface. The spatial content of this motion is typically described by a finite set of Bessel-function based vibration modes below a frequency of interest. To control the vibration modes, it is advantageous to actuate these same shapes for the purpose of attenuation. Perfect surface control would therefore have authority to command both Zernike and vibration mode shapes. This paper provides design criteria for establishing achievable surface deflection performance inside of a "clear aperture" region for a preselected number of desired Zernike polynomials, and a number of retained quasi-statically-actuated vibration mode shapes. The methodology, coined the "modal transformation method" by the authors, is contrasted with a direct projection method in an applied example performed on a MSC.Nastran nonlinear finite element model of a piezoelectric-actuated deformable membrane mirror.**

CONTENTS

IEEEAC paper # 5.0102

I. INTRODUCTION

Spaceborne telescopes, whether used for terrestrial observation or celestial discovery, have their performance ultimately governed by the size of their light-gathering aperture. Future telescopes are envisioned with apertures 10s of meters in diameter. This leap in scale must overcome the packaging limitations that have heretofore restricted today's meter-class mirror diameters. These large telescopes must be designed and fabricated to allow for collapsed packaging which then may be unfurled once in orbit.

This class of collapsible large scale space-based reflectors was outlined by Agnes and Dooley [1] and is proposed by NASA for use in the L2 observatory [2]. The mirror retains it shape primarily by acting as an edge-tensioned membrane, with embedded active elements for fine surface shape control. An artist's conception of a space-based telescope with an annular membrane reflector is shown in Figure 1. The edge-tensioned membrane with active elements is the primary type of structure explored in this structure, although the emphasis is on continuous versus annular circular apertures. Other strategies for pre-straining a mirror include using an intrinsic tension field [3], [4] or pressurizing a lenticular vessel with membrane surfaces [5], [6], [7].

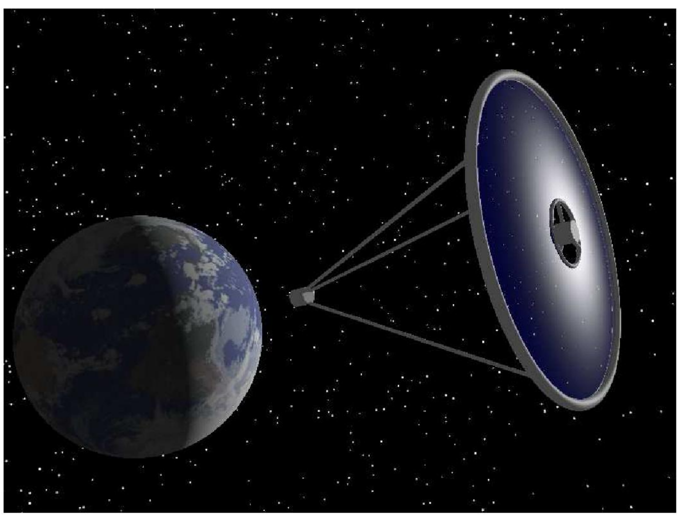

Fig. 1. Artist's conception of a space based telescope *Sobers for the Air Force Institute of Technology, 2002*

Regardless of the tensioning mechanism, the problem of static surface shape control is twofold. The first is ensuring an initially non-aberrated surface, and is a function of both correctly applied initial strain fields and material manufacture. The second problem is quasi-static shape control, particularly the ability of the mirror to act as an active element in an optical system to impart conjugate surfaces, usually expressed in terms of Zernike polynomial basis elements, to correct for known beam-path errors. The displacement functions are often referred to as influence functions. Furthermore, these same influence functions could be used to remove error induced by thermal and/or mechanical loads.

Active quasi-static shape control of circular apertures to produce Zernike polynomial surfaces has been explored by several researchers. A complete review of the Zernike polynomials follows, but for now it suffices to say that Zernike polynomials will always have some displacement at their boundary, while the tensioned membrane structures envisioned in this application are characterized by a fixed, non-displacing, boundary.

Tokovini et al [8] presented the results of a 50-mm 79 actuator electrostatic membrane mirror, where only the interior 35-mm "pupil" was actuated. Although the mirror, which relied on a stiff backing structure, was not scalable to large space structures, the solution methodology of using numerical solutions to Poisson's equation (the governing equation for membrane structures) with an unused "transition zone" between the measured interior area and the boundary show the difficulty of using membrane mirrors to make Zernike shapes. Flint and Denoyer showed the feasibility of using in-plane actuators to produce Zernike polynomial mode shapes on the interior region of a circular membrane mirror [9]. Their results showed the promise of the mirror type, but were tempered by difficulties in computing influence functions due to numerical instabilities. Another observation of Flint and Denoyer's was that the Zernike mode shapes were best observed when the interior 80-90 percent of the circular aperture was utilized for the simulation.

The purpose of this paper is to cast the surface control problem to one in which desired surface shape, expressed in terms of Zernike polynomials, inside of a region we will define as the "clear aperture", can be achieved. The terminology "clear aperture" was used in a figure in a 1977 work by Pearson and Hansen [10] to describe an area on a deformable mirror where data was taken, and thus is similar to our purpose. A notional mirror is displayed in Figure 2 which shows a Zernike tilt surface deflection achieved inside of a clear aperture region in blue.

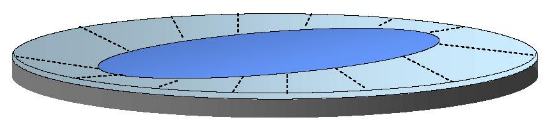

Fig. 2. A notional mirror with a surface tilt deflection achieved inside of the dark blue interior "clear aperture."

To achieve static surface control, an analytic formulation designated by the authors as the *Modal Transformation Method* is developed. A brief outline of the technical development in the paper is summarized here:

- Section II reviews the two commonly-used basis sets to describe a circular aperture. The Zernike polynomial basis set is favored by the optics community, while the Bessel-based vibration mode set is applied to physical solutions of the partial differential equation modelling a tensioned membrane. The fundamental premise of the modal transformation method is casting the problem of obtaining Zernike polynomials using a linear combination of statically-actuated Bessel-function based vibration modes.
- Section III develops the transformation matrices for the radial behavior of the Zernike polynomials and approx-

imated vibration modes in terms of an intermediary radial polynomial basis. The vibration modes must be approximated due to the infinite series representation of the Bessel functions, thus convergence and associated truncation error for a maximum radial polynomial degree is investigated.
- Section IV outlines the modal transformation method. The method is inspired by the projection theorem and an existing analytical relationship between the Zernike polynomials and the Bessel functions. The transformation matrices of the preceding section are combined, and scaled to allow for increased accuracy inside of an interior, clear aperture region. Numeric issues with the transformation matrices are explored.

To show the significance of the methodology, the results are applied to a deformable membrane mirror modelled with finite elements in MSC.Nastran that utilizes piezoelectric in-plane actuation to create changes in surface curvature. Advantages in ease of numerical computation of actuator gains, combined with theoretical a priori knowledge of expected error are shown. Specifically, surface error is shown to be a function of design criterion such as mirror diameter, fineness of actuation grid, and diameter of the clear aperture region, and order of the Zernike mode achieved.

II. Basis Sets for Circular Apertures

Deformable membrane mirrors are employed to form conjugate surfaces to remove atmospheric distortions in an incoming wavefront. For a flat circular aperture, the two-dimensional surface corrections are most often provided in the form of a scaled, truncated set of the Zernike polynomial basis functions. Simultaneously, there exists a requirement in lightweight membrane mirrors to actively resist the dynamic effect which could build at resonance and adversely distort the membrane surface, modelled as a finite set of Bessel-function based vibration modes below a frequency of interest. However, Zernike modes and vibration modes fundamentally differ in that a Zernike mode always has a vertical displacement at the edge, while the vibration mode does not displace vertically from the mirror frame. Pictorial representations for Zernike and vibration modes are provided in Tables I and II respectively.

Inspired by the understanding of the pictorial representation of the two basis functions, we begin this section with a discussion of the mathematical properties and notation associated with the Zernike polynomial, and a matrix representation of the Zernike polynomials is derived. The vibration modes are then reviewed for a circular membrane, and an analogous transformation matrix is created, with the primary difference being that the matrix was formed from an infinite series representation. Next, a direct Zernike to vibration mode transformation is created, both in integral form and then using radial coordinates. Definition of a clear aperture region–an interior region on a circular aperture where Zernike mode shapes will be formed–is then proposed and a series of examples follow.

A. Definition of the Zernike Polynomial

The optics community has used the modified set of Zernike polynomials, as first defined by Noll [11], to describe aberrations in an incoming wavefront. The Zernike polynomials, Z_i, are orthogonal over the interior of the domain of circular aperture of unit radius through the relationship

$$\int_0^{2\pi}\int_0^1 \frac{1}{\pi} Z_i Z_j r\,dr\,d\theta = \delta_{ij} \tag{1}$$

where δ_{ij} is the Kronecker delta. The polynomials, Z_i, are defined as:

$$\left.\begin{aligned} Z_{even j} &= A_n^m R_n^m \cos m\theta, \\ Z_{odd j} &= A_n^m R_n^m \sin m\theta, \end{aligned}\right\} \quad m \neq 0, \tag{2}$$

$$Z_j = A_n^m R_n^m \quad , \quad m = 0. \tag{3}$$

with A_n^m is the normalization constant and R_n^m is the radial polynomial for azimuthal frequency m and radial degree n. The radial polynomial, R_n^m is defined as

$$R_n^m(r) = \sum_{s=0}^{(n-m)/2} \frac{(-1)^s (n-s)!}{s!(m-s)!(n-m-s)!} r^{n-2s} \tag{4}$$

where the values of the azimuthal frequency, m, are less than or equal to the radial degree, n, ($m \leq n$) and $n-m$ is even. The radial polynomials are presented in Table III [11].

The normalization constants, A_n^m, are defined to maintain the orthonormal relationship with respect to the weighted function in Equation 1:

$$A_n^m = \sqrt{2(n+1)}, \qquad m \neq 0, \tag{5}$$

$$A_n^m = \sqrt{(n+1)}, \qquad m = 0. \tag{6}$$

The normalization constants are the coefficients of the terms in Table IV. The Zernike polynomials may be alternately referred to as Zernike mode shapes, recognizing that for the purpose of this document the Zernike mode shapes represent desired surface deflections.

B. Definition of Vibration Modes

While the Zernike mode shapes represent the commanded desired static shapes we wish the circular aperture to obtain, the dynamic motion of the circular membrane is governed by vibration mode shapes. The vibration mode shapes represent the eigenfunctions associated with the natural modes of the system. The vibration mode shapes of the uniform circular membrane of radius ($0 \leq r \leq R$), edge tension T, mass density per surface area ρ, and edge (boundary) condition $w(R,\theta,t) = 0$ may be found by solving the partial differential equation

$$T\nabla^2 w(r,\theta,t) - \rho\ddot{w}(r,\theta,t) = 0 \tag{7}$$

through separation of variables where the separation constant $\lambda = \omega^2$ such that the spatial mode equation is

$$\nabla^2 W(r,\theta) + \beta^2 W(r,\theta) = 0, \qquad \beta = \frac{\rho\omega^2}{T}. \tag{8}$$

Using separation of variables technique to simplify the partial differential equation for the case of a pinned boundary

TABLE I

PICTORIAL REPRESENTATION OF ZERNIKE MODE SHAPES SUCH THAT n = RADIAL DEGREE, m = AZIMUTHAL FREQUENCY.

$n \backslash m$	0	1	2	3	4
0	piston 				
1		tilt 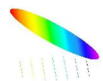			
2	defocus 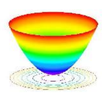		astigmatism 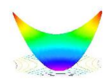		
3		coma 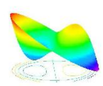		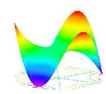	
4	spherical 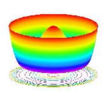		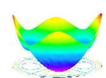		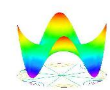

TABLE II

PICTORIAL REPRESENTATION OF VIBRATION MODE SHAPES WITH NORMALIZED NATURAL FREQUENCY ω_{mn} SUCH THAT n = RADIAL DEGREE, m = AZIMUTHAL FREQUENCY.

$n \backslash m$	0	1	2	3	4
1	2.4048 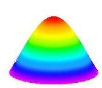	3.8317 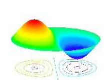	5.1356 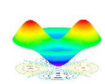	6.3802 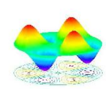	7.5883 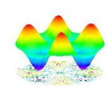
2	5.5201 	7.0156 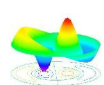	8.4172 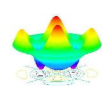	9.7610 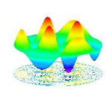	11.0647 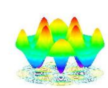
3	8.6537 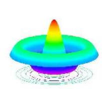	10.1735 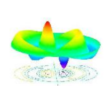	11.6198 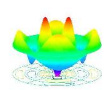	13.0152 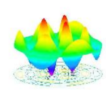	14.3725 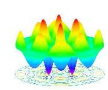
4	11.7915 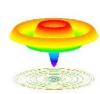	13.3237 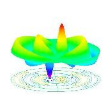	14.7960 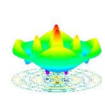	16.2235 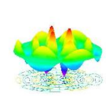	17.6160 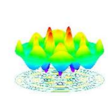

TABLE III

RADIAL POLYNOMIALS R_n^m, n = RADIAL DEGREE, m = AZIMUTHAL FREQUENCY

$n \backslash m$	0	1	2	3	4	5
0	1					
1		r				
2	$2r^2 - 1$		r^2			
3		$3r^3 - 2r$		r^3		
4	$6r^4 - 6r^2 + 1$		$4r^4 - 3r^2$		r^4	
5		$10r^5 - 12r^3 + 3r$		$5r^5 - 4r^3$		r^5
6	$20r^6 - 30r^4 + 12r^2 - 1$		$15r^6 - 20r^4 + 6r^2$		$6r^6 - 5r^4$	
7		$35r^7 - 60r^5 + 30r^3 - 4r$		$21r^7 - 30r^5 + 10r^3$		$7r^7 - 6r^5$
8	$70r^8 - 140r^6 + 90r^4 - 20r^2 + 1$		$56r^8 - 105r^6 + 60r^4 - 10r^2$		$28r^8 - 42r^6 + 15r^4$	
9		$126^9 - 280r^7 + 210r^5 - 60^3 + 5r$		$84r^9 - 168r^7 + 105r^5 - 20r^3$		$36r^9 - 56r^7 + 21r^5$

TABLE IV

ZERNIKE POLYNOMIALS USING NOLL'S ORDERING [11]WHERE R_n^m ARE DEFINED AS IN TABLE III

$n \backslash m$	0	1	2	3	4
0	$Z_1 = R_0^0$ Piston				
1		$Z_2 = 2R_1^1 \cos\theta$ $Z_3 = 2R_1^1 \sin\theta$ Tilt			
2	$Z_4 = \sqrt{3}R_2^0$ Defocus		$Z_5 = \sqrt{6}R_2^2 \sin 2\theta$ $Z_6 = \sqrt{6}R_2^2 \cos 2\theta$ Astigmatism		
3		$Z_7 = \sqrt{8}R_3^1 \sin\theta$ $Z_8 = \sqrt{8}R_3^1 \cos\theta$ Coma		$Z_9 = \sqrt{8}R_3^3 \sin 3\theta$ $Z_{10} = \sqrt{8}R_3^3 \cos 3\theta$	
4	$Z_{11} = \sqrt{5}R_4^0$ Spherical		$Z_{12} = \sqrt{10}R_4^2 \cos 2\theta$ $Z_{13} = \sqrt{10}R_4^2 \sin 2\theta$		$Z_{14} = \sqrt{10}R_4^4 \cos 4\theta$ $Z_{15} = \sqrt{10}R_4^4 \sin 4\theta$
5		$Z_{16} = \sqrt{12}R_5^1 \cos\theta$ $Z_{17} = \sqrt{12}R_5^1 \sin\theta$		$Z_{18} = \sqrt{12}R_5^3 \cos 3\theta$ $Z_{19} = \sqrt{12}R_5^3 \sin 3\theta$	

($W(R,\theta) = 0$), the static mode shapes are obtained. The derivation may be found in a structural dynamics textbook, such as the text by Meirovitch [12]. The mode shapes are

$$W_n^m(r,\theta)_C = B_n^m J_m(\beta_{mn} r) \cos m\theta, \quad \text{m, n = 1, 2, ...} \tag{9}$$
$$W_n^m(r,\theta)_S = B_n^m J_m(\beta_{mn} r) \sin m\theta, \quad \text{m, n = 1, 2, ...} \tag{10}$$
$$W_n^0(r,\theta) = B_n^0 J_0(\beta_{0n} r), \quad \text{n = 1, 2, ...} \tag{11}$$

where

$$B_n^m = \sqrt{\frac{2}{\pi\rho R(J_{m+1}(\beta_{mn} R))}}, \quad \text{m = 1, 2, ...} \tag{12}$$
$$B_n^m = \frac{1}{\sqrt{\pi\rho R(J_1(\beta_{mn} R))}}, \quad \text{m = 0.} \tag{13}$$

The indices m and n represent the azimuthal frequency and radial frequency respectively. The radial frequency is actually the n^{th} zero of the associated m^{th} order Bessel function, and may be thought of as the number of times the Bessel function crosses the radial axis between the center of the membrane and the boundary[1]. The vibration modes of the circular membrane are orthogonal through the relationship

$$\int_0^{2\pi}\int_0^R \rho {W_n^m}_I {W_q^p}_J r dr d\theta = \delta_{IJ}\delta_{mp}\delta_{nq}. \tag{14}$$

[1]The vibration mode shape always satisfies the boundary condition of zero displacement at the boundary through the condition $J_m(\beta_{mn} R) = 0$.

III. MATRIX REPRESENTATIONS OF MODAL TRANSFORMATION

The purpose of this section is to formulate a matrix representation of the radial Zernike polynomial and vibration mode basis sets (note the azimuthal, or angular, behavior is identical for both basis sets). To do that, the radial behavior of each basis set is cast in terms of an intermediary polynomial basis. Since the Bessel function component of the vibration modes consists of an infinite series in the intermediary basis, the resulting modes are therefore an approximation to the vibration modes, subject to truncation error.

A. Zernike Transformation Matrix for a given Azimuthal Frequency

Equation 3 terms $A_m^n R_m^n$ may be written in a summation form where the coefficients are as given in Table III. For a given azimuthal frequency m, the summation will have the form where each row represents the maximum radial degree of the polynomial:

$$
\begin{aligned}
A_n^m R_n^m &= \sum_{k=0}^{N} (a_{2k}^{(m,n)}) r^{2k} r^m, \\
&= (a_0^{(m,n)} + a_2^{(m,n)} r^2 + \dots \qquad (15)\\
&\quad + a_N^{(m,n)} r^{n-m}) r^m, \\
&= \begin{Bmatrix} a_0^{(m,n)} \\ a_2^{(m,n)} \\ \vdots \\ a_N^{(m,n)} \end{Bmatrix}^T \cdot \begin{Bmatrix} 1 \\ r^2 \\ \vdots \\ r^{2N} \end{Bmatrix} r^m. \qquad (16)
\end{aligned}
$$

Furthermore, we can write a series of equations for a given azimuthal frequency m that encompass all radial degrees from m to a maximum degree of n such that

$$
\begin{Bmatrix} A_m^m R_m^m \\ A_m^{m+2} R_m^{m+2} \\ \vdots \\ A_m^{m+2N} R_m^{m+2N} \end{Bmatrix} =
\begin{bmatrix} a_0^{(m,m)} & & & \\ a_0^{(m,m+2)} & a_2^{(m,m+2)} & & \\ & \vdots & \ddots & \\ a_0^{(m,m+2N)} & a_2^{(m,m+2N)} & & a_{2N}^{(m,m+2N)} \end{bmatrix}
\cdot \begin{Bmatrix} 1 \\ r^2 \\ \vdots \\ r^{2N} \end{Bmatrix} r^m \qquad (17)
$$

The Zernike transformation matrix $\boldsymbol{A}_N^m$ may therefore be defined as the lower diagonal transformation matrix of size $N+1 \times N+1$ for an azimuthal frequency m with a maximum polynomial degree $2N+m$ from above. $\boldsymbol{A}_N^m$ is here defined as:

$$
\boldsymbol{A}_N^m \equiv
\begin{bmatrix} a_0^{(m,m)} & & & \\ a_0^{(m,m+2)} & a_2^{(m,m+2)} & & \\ & \vdots & \ddots & \\ a_0^{(m,m+2N)} & a_2^{(m,m+2N)} & & a_{2N}^{(m,m+2N)} \end{bmatrix}. \qquad (18)
$$

B. Vibration Mode Transformation Matrix for a given Azimuthal Frequency

It is our desire to expand the vibration mode shapes from Section II-B. We will accomplish this by creating a vibration mode transformation matrix for a given azimuthal frequency.

To obtain our transformation matrix, begin by writing the series representation of the Bessel functions in terms of bookkeeping coefficients $\alpha_{2k}^{(m,n)}$:

$$
\begin{aligned}
&J_m(\beta_{mn} r) = \\
&(\frac{1}{2}\beta_{mn} r)^m \sum_{k=0}^{\infty} \frac{(-1)^k (\frac{1}{2}\beta_{mn} r)^{2k}}{(k+m)!k!}, \qquad (19)\\
&= \sum_{k=0}^{\infty} \alpha_{2k}^{(m,n)} r^{2k+m}, \qquad (20)\\
&= (\alpha_0^{(m,n)} + \alpha_2^{(m,n)} r^2 + \dots) r^m, \qquad (21)\\
&= \begin{bmatrix} \alpha_0^{(m,n)} & \alpha_2^{(m,n)} & \dots \end{bmatrix} \begin{Bmatrix} 1 \\ r^2 \\ \vdots \end{Bmatrix} r^m. \qquad (22)
\end{aligned}
$$

Next, we apply the vibration mode shape normalization coefficients from Equations 12 and 13 such that $b_{2k}^{(m,n)} = B_n^m \alpha_{2k}^{(m,n)}$, we arrive at

$$
\begin{aligned}
B_n^m J_m(\beta_{mn} r) &= \sum_{k=0}^{\infty} (b_{2k}^{(m,n)}) r^{2k} r^m, \\
&= \begin{bmatrix} b_0^{(m,n)} & b_2^{(m,n)} & \dots \end{bmatrix} \begin{Bmatrix} 1 \\ r^2 \\ \vdots \end{Bmatrix} r^m \qquad (23)
\end{aligned}
$$

We desire to write a transformation matrix analogous to Equation 18 for a given azimuthal frequency m. Therefore, we construct a series of equations from Equation 23 such that

$$
\begin{Bmatrix} B_1^m J_m(\beta_{m1} r) \\ B_2^m J_m(\beta_{m2} r) \\ \vdots \end{Bmatrix} =
\begin{bmatrix} b_0^{(m,1)} & b_2^{(m,1)} & \dots \\ b_0^{(m,2)} & b_2^{(m,2)} & \dots \\ & \vdots & \ddots \end{bmatrix} \begin{Bmatrix} 1 \\ r^2 \\ \vdots \end{Bmatrix} r^m. \qquad (24)
$$

We then construct a series of $N+1$ equations and truncate the approximations to a maximum radial polynomial degree of $2N+m$. The equations are

$$
\begin{Bmatrix} B_1^m J_m(\beta_{m1} r) \\ B_2^m J_m(\beta_{m2} r) \\ \vdots \\ B_{N+1}^m J_m(\beta_{m(2N)} r) \end{Bmatrix} \approx
\begin{bmatrix} b_0^{(m,1)} & b_2^{(m,1)} & \dots & b_{2N}^{(m,1)} \\ b_0^{(m,2)} & b_2^{(m,2)} & \dots & b_{2N}^{(m,2)} \\ & \vdots & & \ddots \\ b_0^{(m,N+1)} & b_2^{(m,N+1)} & \dots & b_{2N}^{(m,N+1)} \end{bmatrix}
\cdot \begin{Bmatrix} 1 \\ r^2 \\ \vdots \\ r^{2N} \end{Bmatrix} r^m. \qquad (25)
$$

From Equation 25, we define our $N+1 \times N+1$ vibration modal transformation matrix, $\boldsymbol{B}_N^m$ as such,

$$B_N^m \equiv \begin{bmatrix} b_0^{(m,1)} & b_2^{(m,1)} & \dots & b_{2N}^{(m,1)} \\ b_0^{(m,2)} & b_2^{(m,2)} & \dots & b_{2N}^{(m,2)} \\ \vdots & & \ddots & \\ b_0^{(m,N+1)} & b_2^{(m,N+1)} & \dots & b_{2N}^{(m,N+1)} \end{bmatrix}. \tag{26}$$

The invertibility of the matrix B_N^m is discussed in Section IV-D. Furthermore, the Bessel terms in Equation 25 will only be correctly represented to the precision of the next section.

C. Convergence of the Bessel (Alternating) Series and Associated Truncation Error

Our goal is to be able to transform information of the surface deformation from our Zernike subspace to vibration modal coordinates and vice-versa. To write the Zernike polynomials in terms of the modal coordinates, we will need a finite expression of the Bessel functions in our intermediate coordinate system of radius and azimuthal angle.

By definition the Bessel functions may be written as the series [13]

$$J_m(\beta_{mn}r) = (\frac{1}{2}\beta_{mn}r)^m \sum_{k=0}^{\infty} \frac{(-1)^k(\frac{1}{2}\beta_{mn}r)^{2k}}{(k+m)!k!}. \tag{27}$$

For the symmetric modes, m = 0, and Equation 27 may be reduced to

$$J_0(\beta_{0n}r) = \sum_{k=0}^{\infty} \frac{(-1)^k(\frac{1}{2}\beta_{0n}r)^{2k}}{k!^2}. \tag{28}$$

For instance, the first zero of $J_0(\beta R) = 0$ is $\beta_{01} = \frac{2.4048}{R}$ and the infinite summation where $\tilde{r} \equiv \frac{r}{R}$:

$$J_0(2.4048\tilde{r}) = 1 - 1.4458\tilde{r}^2 + 0.52258\tilde{r}^4 + O(\tilde{r}^6). \tag{29}$$

Returning to the general case of any non-negative integer m, to accomplish our desired transformation, we must approximate the Bessel functions by a truncated series. We note here that in the future sections we will relate the Zernike modes with the Bessel-based vibration modes. The two basis sets have exactly the same azimuthal behavior. Thus, it is error in the radial terms that will contribute to overall error in the relationship.

To this end, the degree of truncation is estimated to ensure accuracy to within some approximation tolerance, ϵ.

Begin by defining

$$B_m^\kappa(\beta_{mn}r) \equiv \sum_{k=0}^{\kappa-1} \frac{(-1)^k(\frac{1}{2}\beta_{mn}r)^{2k+m}}{(k+m)!k!} \tag{30}$$

where again $\tilde{r} \equiv \frac{r}{R}$. From this point we will drop the tilde, realizing that our r is a normalized value. Note this is simply the first κ terms of the Bessel series.

Next, choose κ such that

$$\left|J_m(\beta_{mn}r) - B_m^\kappa(\beta_{mn}r)\right| < \epsilon. \tag{31}$$

Because the Bessel function is an alternating series the error in truncating the series is no worse than the first term neglected, that is

$$\left|J_m(\beta_{mn}r) - B_m^\kappa(\beta_{mn}r)\right| \le \frac{(\frac{1}{2}\beta_{mn}r)^{2\kappa+m}}{(\kappa+m)!\kappa!}. \tag{32}$$

Further, because $m \ge 0$ we have

$$\frac{(\frac{1}{2}\beta_{mn}r)^{2\kappa+m}}{(\kappa+m)!\kappa!} < \frac{(\frac{1}{2}\beta_{mn}r)^{2\kappa+m}}{(\kappa!)^2}. \tag{33}$$

For large values of κ, Stirling's formula may be used to simplify large values of the factorial expression $\kappa!$:

$$\kappa! \approx \kappa^\kappa e^{-\kappa}\sqrt{2\pi\kappa} \tag{34}$$

Applying Stirling's formula, the magnitude of the error becomes

$$\frac{e^{2\kappa}(\frac{1}{2}\beta_{mn}r)^{2\kappa+m}}{2\pi\kappa^{2\kappa+1}} < \epsilon. \tag{35}$$

Upon further simplification, our error bound formula is

$$\frac{(\frac{1}{2}\beta_{mn}r)^m}{2\pi\kappa}\left(\frac{e\beta_{mn}r}{2\kappa}\right)^{2\kappa} < \epsilon. \tag{36}$$

This truncation error represents an error bound on the radial portion of the truncated modes. In future constructs, when approximating Bessel functions, enough terms should be chosen so that this error is negligible.

IV. Modal Transformation Method for Circular Apertures

In this section, a method is developed which allows Zernike surfaces to be projected on an interior region of a circular aperture by a linear combination of Bessel-based vibration mode shapes. In short, by comprising a desired optical surface in terms of physically realizable mode shapes, steady-state surface control should be readily achievable.

A. Projection of the Zernike Modes onto the Vibration Modes

The Zernike polynomials of Section II-A are related to the Bessel function of the first kind by the formula presented by Noll [11]:

$$R_n^m(r) = 2\pi(-1)^{(n-m)/2}\int_0^\infty J_{n+1}(2\pi\xi)J_m(2\pi\xi r)d\xi. \tag{37}$$

Therefore, we expect it is reasonable to express Zernike mode shapes in terms of vibration mode shapes. To do so, we'll develop an approach based upon the orthogonal properties of the two basis sets and the projection theorem.

B. Existing Analytical Relationship

To define a Zernike mode in terms of a vibration mode, let's look at the case of the axisymmetric modes first. We desire

$$Z_i = \sum_{n=0}^{\infty} c_n^{(i)} W_n^0. \tag{38}$$

Therefore, we may write (assuming both mode shapes have been normalized to the same unit radius)

$$c_n^{(i)} = \frac{\int_0^{2\pi}\int_0^1 \frac{1}{\sqrt{\pi}} Z_i(r) W_n^0(r) r dr d\theta}{\int_0^{2\pi}\int_0^1 (W_n^0(r))^2 r dr d\theta} \tag{39}$$

noting there is no dependence on θ such that the azimuthal integral term is replaced by the quantity 2π. The term $\frac{1}{\sqrt{\pi}}$ is required because Noll's scheme as presented in Equation 1 requires a linear weighting, which in our relationships is equally distributed among the Zernike modes. Further note the vibration modes are already normalized, thus Equation 39 reduces to

$$c_n^{(i)} = 2\pi \int_0^1 \frac{1}{\sqrt{\pi}} Z_i(r) W_n^0(r) r dr. \tag{40}$$

Substituting the results of mode shape Equations 11 and 13 with unit density (and $R = 1$) yields

$$c_n^{(i)} = \frac{2}{J_1(\beta_{0n})} \int_0^1 Z_i J_0(\beta_{0n} r) r dr. \tag{41}$$

The approximation of the piston Zernike mode using Equation 38 through Equation 41 arbitrarily truncated at 40 terms (axisymmetric modes) is presented in Figure 3.

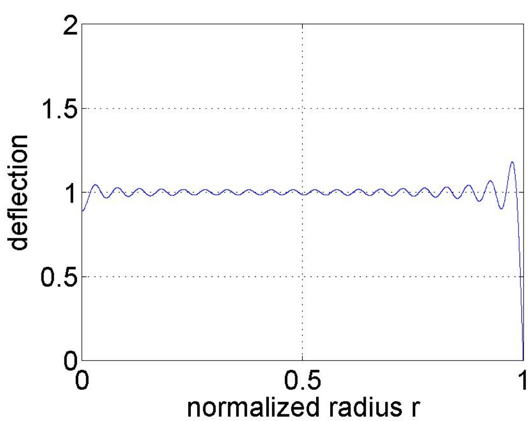

Fig. 3. Piston Zernike mode (Z_1) approximated by a linear combination of the first 40 axisymmetric vibration mode shapes.

From this section, we make the following observations. In Figure 3, even with a linear combination of 40 mode shapes, we observe nearly 20 per cent error at a normalized radius of 0.9-1.0. Also, the representation is computationally intensive due to numeric integration. Thus, we seek a simpler solution where integration is avoided, and a bound on relative error may be forecast.

C. Zernike to Vibration Mode Matrix Transformation

While Equation 38 allows the Zernike modes to be written in the form of integral equations, we may alternately apply the results of Sections III-A and III-B to write an approximate modal transformation. Begin by defining a vector of Zernike and vibration modes for a given frequency for radial degrees up to $2N$. For simplicity, we define the axisymmetric case:

$$\boldsymbol{Z}_0 = \begin{Bmatrix} R_0^0 \\ \sqrt{3}R_2^0 \\ \vdots \\ \sqrt{2N+1}R_{2N}^0 \end{Bmatrix} = \boldsymbol{A}_N^0 \begin{Bmatrix} 1 \\ r^2 \\ \vdots \\ r^{2N} \end{Bmatrix}, \tag{42}$$

and

$$\boldsymbol{W}_0 = \begin{Bmatrix} W_1^0 \\ W_2^0 \\ \vdots \\ W_{N+1}^0 \end{Bmatrix} = \boldsymbol{B}_N^0 \begin{Bmatrix} 1 \\ r^2 \\ \vdots \\ r^{2N} \end{Bmatrix}. \tag{43}$$

Solve for radial vector, $\{1, r^2, \ldots, r^{2N}\}^T$ in Equation 43:

$$\begin{Bmatrix} 1 \\ r^2 \\ \vdots \\ r^{2N} \end{Bmatrix} = (\boldsymbol{B}_N^0)^{-1}\boldsymbol{W}_0, \tag{44}$$

and then substitute into Equation 42 to yield the expression:

$$\boldsymbol{Z}_0 = \boldsymbol{A}_N^0(\boldsymbol{B}_N^0)^{-1}\boldsymbol{W}_0. \tag{45}$$

Through a similar manner write the non-axisymmetric equations:

$$\boldsymbol{Z}_{\boldsymbol{S}m} = \boldsymbol{A}_N^m(\boldsymbol{B}_N^m)^{-1}\boldsymbol{W}_{\boldsymbol{C}m}, \tag{46}$$

$$\boldsymbol{Z}_{\boldsymbol{C}m} = \boldsymbol{A}_N^m(\boldsymbol{B}_N^m)^{-1}\boldsymbol{W}_{\boldsymbol{S}m}, \tag{47}$$

where the modal vectors of length $N+1$ are composed of modes of axisymmetric mode shapes ($\boldsymbol{Z_0}$,$\boldsymbol{W_0}$), modes with cosine angular dependence of frequency m ($\boldsymbol{Z}_{\boldsymbol{C}m}$, $\boldsymbol{W}_{\boldsymbol{C}m}$), and modes with sine angular dependence of frequency m ($\boldsymbol{Z}_{\boldsymbol{S}m}$, $\boldsymbol{W}_{\boldsymbol{S}m}$).

D. Near Singularity of the Modal Transformation Matrix

The modal transformation matrix, $\boldsymbol{B}_N^m$, is most conveniently applied by defining it as a square matrix in Section III-B, so that its inverse in Section IV-C is unique. Non-square issues addressed with the pseudo-inverse are not included herein.

The size of $\boldsymbol{B}_N^m$ is determined by the number of (or highest degree) of vibration modes the designer will be able to actuate–those modes are essentially dependent on the fineness of the actuator grid. The value of N should be large enough so that actuated modes are represented with a small to negligible truncation error as derived in Equation 36. However, the resulting ($\boldsymbol{B}_N^m$) is ill-conditioned, and is not readily invertible for large values of N. A method for decomposing the matrix into a diagonal matrix $\tilde{\boldsymbol{N}}$ and remaining components $\tilde{\boldsymbol{B}}_N^m$ was applied to allow inversion on 32-bit processors for values of $N \leq 20$.

Begin by defining:

$$\boldsymbol{B}_N^m \equiv \tilde{\boldsymbol{N}} \tilde{\boldsymbol{B}}_N^m \tag{48}$$

where the diagonal elements of $\tilde{\boldsymbol{N}}$ are defined as

$$\tilde{N}_{ii} = (B_N^m)_{ii} \tag{49}$$

.

The remaining off-diagonal elements of $\tilde{\boldsymbol{N}}$ are zero. Thus constructed, much of the ill-conditioned nature of $\boldsymbol{B}_N^m$ is shifted to $\tilde{\boldsymbol{N}}$, for which an analytical inverse readily exists.

As a simple example, for the case where $N = 2$ and $m = 0$, ρ and R are normalized to 1, and the factor $\frac{1}{\sqrt{\pi}}$ is removed, the matrices are:

$$\boldsymbol{B}_N^m = \begin{bmatrix} 1.0868 & -1.5712 & 0.5679 \\ -1.6581 & 12.6310 & -24.0552 \\ 2.0784 & -38.9115 & 182.1229 \end{bmatrix}, \tag{50}$$

$$\tilde{\boldsymbol{N}} = \begin{bmatrix} 1.0868 & 0 & 0 \\ 0 & 12.6310 & 0 \\ 0 & 0 & 182.1229 \end{bmatrix}, \tag{51}$$

$$\tilde{\boldsymbol{B}}_N^m = \begin{bmatrix} 1.0000 & -1.4458 & 0.5226 \\ -0.1313 & 1.0000 & -1.9045 \\ 0.0114 & -0.2137 & 1.0000 \end{bmatrix}. \tag{52}$$

In this example, the original condition number of $\boldsymbol{B}_N^m$ is reduced from 240.9 to 21.3 while the condition number of $\tilde{\boldsymbol{N}}$ is 167.5831, of little impact due to the ease of inverting $\tilde{\boldsymbol{N}}$ analytically, allowing $(\boldsymbol{B}_N^m)^{-1} = (\tilde{\boldsymbol{N}})^{-1}(\tilde{\boldsymbol{B}}_N^m)^{-1}$.

E. Defining a Clear Aperture Control Region

To this point, every effort made has focused on projecting a Zernike space onto a Bessel-based vibration mode space. A valiant effort, yet one that will prove frustrating due to the incompatibility of the boundary conditions for these competing basis sets. To avoid this inherent difficulty, it is proposed to define a *clear aperture* region as a subspace of the Bessel-based vibration mode space. Simply stated, the clear aperture region will be a circular region with some radius $a < R$, as was first introduced in Figure 2. Defining the scaled variable $\hat{r} = r/a$ for the Zernike polynomials in this subspace, and noting that on the clear aperture boundary $\hat{r} = 1$, we relate the polynomial vector, $\{1, \hat{r}^2, \ldots, \hat{r}^{2N}\}$to the radial vector $\{1, r^2, \ldots, r^{2N}\}$ with the diagonal matrix $\boldsymbol{S}_N^m$. The matrix $\boldsymbol{S}_N^m$ is

$$\boldsymbol{S}_N^m = \frac{1}{a^m} \begin{bmatrix} 1 & & & \\ & \frac{1}{a^2} & & \\ & & \ddots & \\ & & & \frac{1}{a^{2N}} \end{bmatrix} \tag{53}$$

such that

$$\begin{Bmatrix} 1 \\ \hat{r}^2 \\ \ldots \\ \hat{r}^{2N} \end{Bmatrix} \hat{r}^m = [S] \begin{Bmatrix} 1 \\ r^2 \\ \ldots \\ r^{2N} \end{Bmatrix} r^m. \tag{54}$$

Again, as in previous sections, the transformation matrix is for an azimuthal frequency m with a maximum polynomial degree $2N+m$. For Zernike shape control of the clear aperture region, the governing equations, Equations 45 - 47 scale to become

$$\boldsymbol{Z}_0 = \boldsymbol{A}_N^0 \boldsymbol{S}_N^0 (\boldsymbol{B}_N^0)^{-1} \boldsymbol{W}_0, \tag{55}$$

$$\boldsymbol{Z}_{\boldsymbol{S}m} = \boldsymbol{A}_N^m \boldsymbol{S}_N^m (\boldsymbol{B}_N^m)^{-1} \boldsymbol{W}_{\boldsymbol{C}m}, \tag{56}$$

$$\boldsymbol{Z}_{\boldsymbol{C}m} = \boldsymbol{A}_N^m \boldsymbol{S}_N^m (\boldsymbol{B}_N^m)^{-1} \boldsymbol{W}_{\boldsymbol{S}m}. \tag{57}$$

F. Application of Modal Transformation Method

With the underlying theory thus provided, a series of specific application of the modal transformation method for circular apertures is presented to show the applicable design criterion for deformable mirrors.

To begin, the method is compared to the projection theorem used in Section IV-A. In Figure 4, the radial behavior of a surface composed of the first 10 axisymmetric vibration mode shapes is constructed to approximate the axisymmetric Defocus Zernike mode, $Z_4 = \sqrt{3}(2r^2 - 1)$ over the entire surface (effectively, the clear aperture as previously presented is one). In Figure 4(a), the representation is constructed using coefficients from the projection theorem, and in Figure 4(b), the coefficients were generated using the modal transformation method for N = 20. The error between the desired Zernike surface and the vibration modal representation was calculated using the discretized weighted Euclidean norm[2] (the plots were calculated using 10^4 points).

With the clear aperture thus set to one, the projection theorem results in the smaller error between the desired surface and its modal representation ($Error = 0.2407$ versus $Error = 0.3604$), and of course is the best achievable performance. However, the shape of the modal surface in Figure 4(a) has evidence of distortion throughout its surface, while Figure 4(b) shows significant distortion only at the outer edge to meet the boundary condition.

Next, in Figure 5, the clear aperture is adjusted to values less than one, and the Defocus Zernike mode is constructed as before in Figure 4 using the modal transformation method.

[2]The discretized weighted Euclidean norm $\|\cdot\|_\Delta$ in cylindrical coordinates for radial grid spacing Δr and azimuthal spacing $\Delta\theta$ is

$$\|\boldsymbol{f} - \boldsymbol{g}\|_\Delta = \Big(\Delta r \Delta\theta \sum_{i=1}^{N} r_i [f_i(r_i, 2\pi\theta_i) - g_i(r_i, 2\pi\theta_i)]^2\Big)^{\frac{1}{2}}. \tag{58}$$

Assuming a circular domain with unit radius, this limit of the vector norm as the step size decreases yields the functional 2-norm:

$$\lim_{\Delta r, \Delta\theta \to 0} \|\boldsymbol{f} - \boldsymbol{g}\|_\Delta = \Big(\int_0^{2\pi} \int_0^1 [f - g]^2 r dr d\theta\Big)^{\frac{1}{2}} = \|f - g\|_2. \tag{59}$$

This result will give us a stable error term to use. Compare this norm to the familiar Root Mean Square error, which does not account for the weighting factor r_i, and does not readily account for differing grid spaces on orthogonal axes within the vectors themselves:

$$E_{RMS} \equiv \frac{1}{N}\Big(\sum_{i=1}^{N} [f_i - g_i]^2\Big)^{\frac{1}{2}}. \tag{60}$$

Further note that in some cases presented only radial error is reported, and thus the azimuthal terms (θ dependence) is not required.

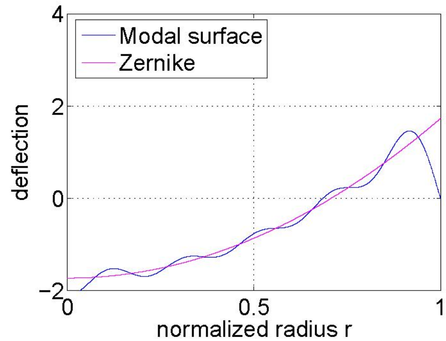

(a) Projection theorem. Error norm 0.2407.

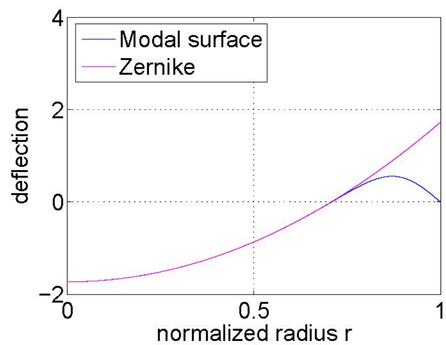

(b) Modal transformation (N=20). Error norm 0.3604.

Fig. 4. Comparison of modal representations of the axisymmetric Defocus Zernike radial behavior using the first 10 axisymmetric vibration modes.

In Figures 5(a)-(c), the radial behavior is plotted for clear apertures of 0.7, 0.8 and 0.9. It is quite apparent that for clear aperture of 0.7, the deviation between the desired Zernike shape and the modal surface is indistinguishable at the scale shown.

Base 10 log of the error for clear apertures between 0.1 and 1 is presented in Figure 5(d). For this specific example, the error was at a minimum for clear aperture of $a = 0.67$, the location of which was invariant when a finer increment in the vector was chosen and evaluated. Identifying the location of minimum error in general terms is an area of further investigation.

With the clear aperture set at 0.7, another series of plots was constructed for Figure 6, again using the modal transformation method for $N = 20$. For these plots, the variable was the number of axisymmetric vibration modes that were used to construct the desired Defocus Zernike mode, and a overall plot of error for 5 through 20 actuated modes is presented in Figure 6(d). Note that for the modal transformation matrix, the value of N caps the number of actuated modes which may be used. The use of one to four modes was calculated, but errors in excess of 0.1 were off-scale for the plot provided. For this example, the error decreased steadily until $n = 10$, and then remained steady. It is hypothesized that this error is due to the truncation error of the approximated vibration mode, a function of Equation 36. Relation of the truncation error to the number of actuated modes is an area of investigation.

For the structural engineer, these results may be transformed into design criterion for construction of a deformable mirror. Beginning with a desired optical surface error budget and a desired radius of the aperture region, the engineer may choose to actuate a greater number of vibration modes or reduce the clear aperture to achieve the desired performance. Actuating the number of modes (within the error budget) will be limited by the fineness of the available surface actuators and computing and energy requirements. With a fixed reflective area predefined, decreasing the clear aperture will effectively increase the radius of the overall structure, with whatever associated weight penalties that entails. However, it is aptly demonstrated that setting a clear aperture region to an arbitrary value, such as eighty percent, is neglecting the design optimization that could be performed by the engineer.

V. Example: Finite Element Model

In this section, the techniques developed are applied to a finite element model of a piezoelectric actuated deformable mirror. The finite element model is a simplified version of experimental hardware under development at the Air Force Institute of Technology (AFIT). Experimental results of versions of the mirror have been reported on previously [14], [15]. The current AFIT deformable mirror testbed is a circular 5-inch laminar composite structure with a piezoelectric actuating layer of polyvinylidene fluoride (PVDF), a substrate of silicone, and a near-optical quality reflective layer of gold. An electrode pattern comprised of seven actuators is etched onto the PVDF film. Voltage induces a strain in the piezoelectric layer offset from the neutral axis, termed in-plane actuated unimorph actuation, a visual depiction of which is shown in Figure 7. The experimental hardware is pictured in Figure V.

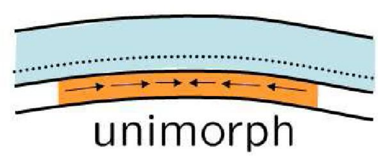

Fig. 7. Unimorph actuation occurs when an actuating layer offset from the neutral axis contracts or expands and thus induces a surface curvature. In the AFIT deformable mirror, the actuating layer in orange is PVDF material, and the substrate in blue is silicone.

Future developments of the experimental hardware include the refinement of the actuator electrode pattern from seven to 61 actuating regions. A 61-actuator region is sufficient to show the validity of the control algorithms presented in this paper. In lieu of experimental data, a high-order finite element model of the AFIT deformable mirror was chosen to provide simulated results.

A. MSC.Nastran Finite Element Model

A finite element model of the the AFIT deformable mirror testbed was created in MSC.Nastran. The model used the same dimensions of the experimental hardware, except instead of seven actuating regions, the surface was divided into 61 regions. The 3601 node model was comprised of 3384 CQUAD4 elements and 72 CRIA3 composite plate

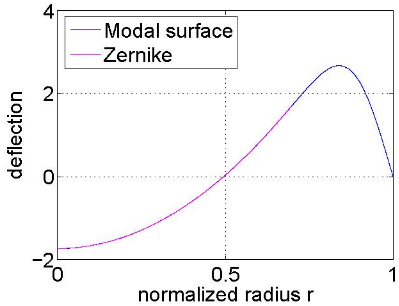

(a) Clear aperture $= 0.7$.

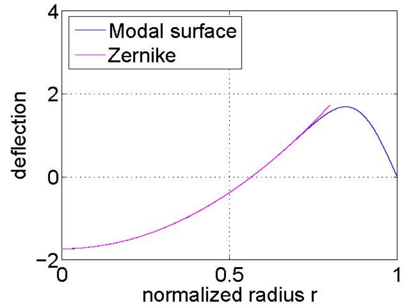

(b) Clear aperture $= 0.8$.

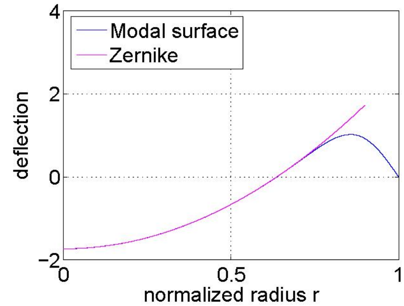

(c) Clear aperture $= 0.9$.

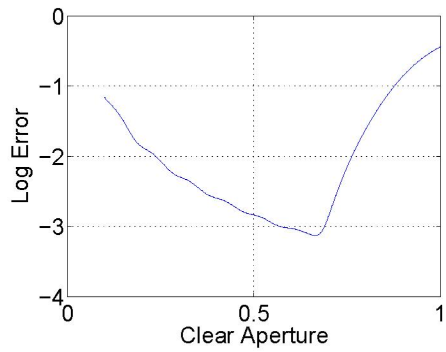

(d) Log10(Error) versus clear aperture.

Fig. 5. Impact of Clear Aperture on representation of the Defocus Zernike by the first 10 axisymmetric vibration modes using the modal transformation for N = 20. Figure 5(d) shows the error throughout the range of clear aperture settings, which for this case was at a minimum when $a = 0.67R$.

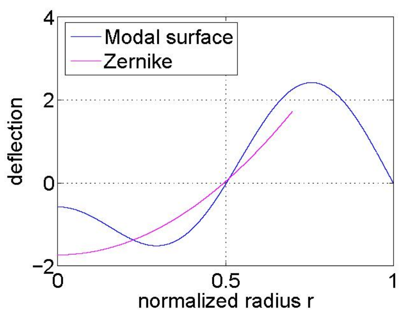

(a) $k = 3$.

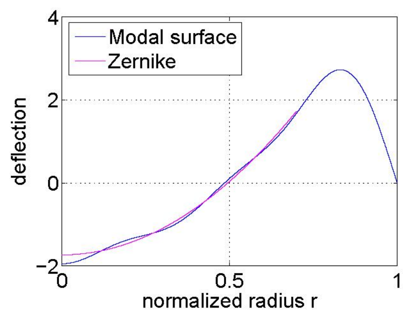

(b) $k = 6$.

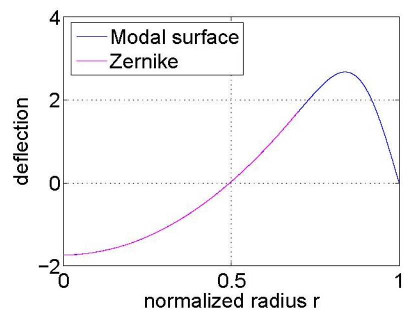

(c) $k = 10$.

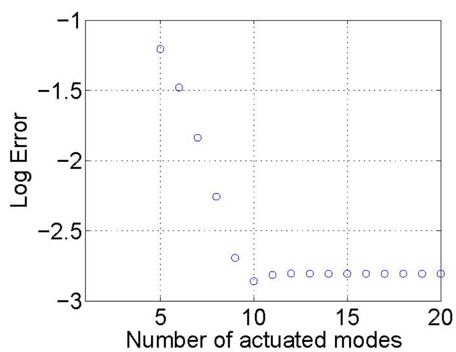

(d) Log10(Error) versus number of actuated vibration modes.

Fig. 6. Impact on representation of Defocus Zernike by varying the number axisymmetric vibration modes (k) using the modal transformation for N = 20 and Clear Aperture = 0.7. Figure 6(d) shows the error for 5 to 20 vibration modes.

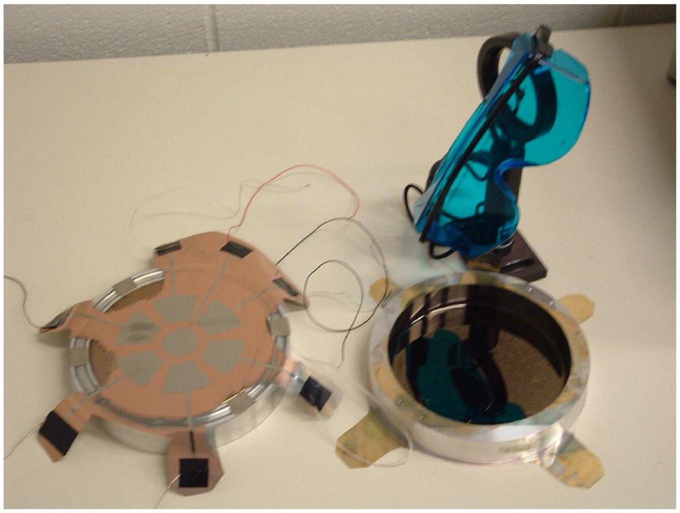

Fig. 8. AFIT deformable mirror test articles. The mirrors are 5-inch, solid aluminum framed structures with reflective gold, silicone, and PVDF layers forming the active face. The 7-actuator electrode pattern is clearly visible on the left mirror, which is viewed from the back (non-reflective) side. A pair of blue, eye-protection goggles provides a sense of scale.

elements. The substrate and actuating layers were modelled, while the gold reflective layer and copper-nickel electrode layers were considered negligible. Piezoelectric forcing was introduced using the linear piezoelectric-thermal analogy [16] at the locations in Table V. For the purposes of this example, the directionality of the piezoelectric dielectric constants was removed. Material properties are presented in Table VI.

TABLE V

ACTUATOR LOCATIONS FOR 61-ACTUATOR, 0.0624 M RADIUS MODEL.

inner radius (m)	outer radius (m)	number of azimuthal divisions	degrees per division
N/A	0.0071	1	360
0.0071	0.0212	6	60
0.0212	0.0353	12	30
0.0353	0.0494	18	20
0.0494	0.0622	24	15

TABLE VI

MATERIAL PROPERTIES

Parameter	Silicone	PVDF	Units
Young's modulus	1.013	4000	$10^6 N/m^2$
Poisson's ratio	0.497	0.3	
d_{31}	N/A	23	$10^{-12} \frac{m/m}{V/m}$ or $\frac{C/m^2}{N/m^2}$
thickness	.0015	$52.0E{-6}$	m

A uniform edge tension was applied using an enforced displacement boundary condition in the radial direction. Then, using a non-linear static solution, the stiffness of the model was updated, and an equivalent thermal load was introduced to simulate voltage application at the various actuator locations.

The out-of-plane surface displacements were extracted for analysis. Zernike coefficients were calculated for the area inside of the clear aperture, which could then be used to formulate conclusions about the behavior of various control methodologies.

B. Static Control Methodology for Membrane Mirrors

To provide a competing methodology for computing actuation voltages for static surface control of the Zernike polynomials and calculate the vibration mode shapes in this region, the deformable mirror was modelled as a fixed boundary membrane structure. The forcing functions were modelled consistent with existing smart structure theory, where the piezoelectric loads are simply line moments acting along the actuator boundary. For a complete derivation of the theory, the reader is referred to Nayfeh and Pao's text [17]. With plate and non-linear in-plane tension effects neglected, the governing equation for the deformable mirror with J actuators is:

$$T\nabla^2 w(r,\theta) = M\nabla^2 \sum_{i=1}^{J} F_i(r,\theta), \tag{61}$$

where

$$M = \frac{E}{1-\nu}\frac{d_{31}}{t}(-\frac{1}{2})hV_i. \tag{62}$$

In the above equation, T is membrane tension, E is the substrate modulus, ν is the substrate Poisson's constant, d_{31} is the piezoelectric constant, t is the thickness of the piezoelectric layer, h is the thickness of the substrate layer, and V_i is the voltage across the electrodes. Note that we have assumed a negligible structural contribution of the piezoelectric layer to the deformation of the surface.

For our example, F_i is the area of electrode as shown in Figure 9. The i^{th} region may be defined through heaviside functions with radial boundaries ξ_i^U and ξ_i^L and azimuthal boundaries ϕ_i^U and ϕ_i^L :

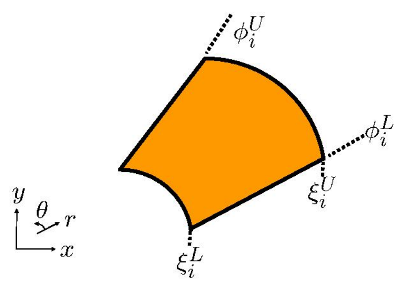

Fig. 9. i^{th} actuator boundaries from Equation 63.

$$F_i(r,\theta) = \{H(r-\xi_i^L)-H(r-\xi_i^U)\}\cdot\{H(\theta-\phi_i^L)-H(\theta-\phi_i^U)\}. \tag{63}$$

Therefore, it is quite obvious that solutions to the partial differential equation are simply a series of scaled step functions corresponding to the applied voltage on the actuated electrode. We later take advantage of the orthogonal nature of the solution. For a unit voltage, these shapes are defined here as Ψ_i modes. To obtain a desired shape on the membrane surface, it is simply a matter of using the projection theorem to find the individual actuator gains.

For the direct projection method of control, the desired Zernike is constructed directly from the Ψ mode shapes. In the proposed modal transformation method, the Ψ mode shapes are actuated to replicate the membrane vibration mode shapes, and then the transformation constructs the desired Zernike surface on the clear aperture region using linear combinations of the approximated vibration mode shapes. Again, it is emphasized that the modal transformation method always satisfies the fixed edge boundary conditions, and further limits steep transitions if the Zernike modes are implemented on the interior clear aperture region.

C. Static Control Simulation and Results

In the simulation example, voltages were applied to the MSC.Nastran non-linear finite element model. The desired shape was a simultaneous surface deflection corresponding to the axisymmetric Zernike defocus mode and the non-axisymmetric tilt mode associated with $cos(\theta)$. The clear aperture region was set to 0.78, inside the boundary of the last ring of actuators. A logic flow chart depicts these operations in Figure 10. In this modal transformation method, the value of N was set to 20, and the number of actuated vibration modes at a given azimuthal frequency was limited to five. This limit corresponded to the number of actuation "rings", and thus the maximum number of zero crossings that was theoretically obtainable. The value of N ensured the truncation error of Equation 36 would be negligible.

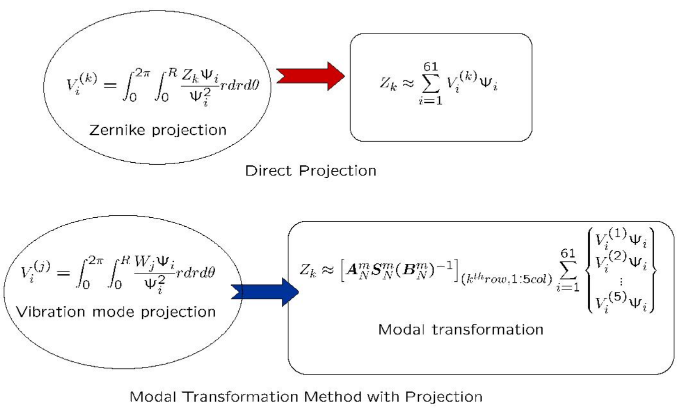

Fig. 10. Pseudocode for computing the voltages in Figure 11(a) and (d). In the direct projection method, the Zernike shapes are constructed in the clear aperture from a linear combination of the actuator (Ψ) modes. In this application of the modal transformation method, the vibration mode shapes are approximated using the projection theorem to form linear combinations of actuator modes, and then those shapes are used in the modal transformation method algorithm. In the figure, indices i correspond to actuator mode, j to vibration mode, and k to desired Zernike surface.

The voltage inputs, finite element model simulation results, and absolute error between the desired surface and the simulated surface are provided for both the direct projection and modal transformation method in Figure 11.

When calculating the voltage inputs for the 61 actuation regions in Figure 11(a) and (d), there was a scaling issue between the chosen mode shapes. The scaling issue existed for both methods, however, it was not the same. Therefore, the input voltages were scaled in each method to produce consistent coefficients between the defocus and tilt modes. The scaling coefficients for the defocus mode were 0.6366 for the modal transformation method, and 0.7518 for the direct projection method. All other responses were linear for the micron level surface displacements in this simulation corresponding to input voltages between -500 to 500 Volts (the practical limit for PVDF material).

The surface deflection and error plots are compared in the remaining plots of Figure 11. To calculate surface error the desired defocus and tilt coefficients were subtracted from the generated surface inside of the clear aperture region, *as well as the piston mode*. The removal of the piston term is of no consequence in optical systems as it is generally not measurable nor does it affect the mirror's optical performance.

While the absolute error plots in Figure 11 give some idea of the performance achievable using the modal transformation method, a break down of the surface terms by Zernike coefficients is presented in Figure 12(a) and (b). In both graphs, the desired (and achieved) Zernike coefficient was normalized for approximately 1×10^{-6} to one. The next three Zernike coefficients for next three higher radial order at the same azimuthal frequency were then normalized and plotted. The coefficients (and thus contribution to the error) for the $\sin$ terms and the higher azimuthal frequency terms (such as $\cos 2\theta, \cos 3\theta, etc$) were not significant and thus are not presented (except in the absolute error plots of Figure 11).

When comparing the modal transformation method with the direct projection method in Figure 12(a) and (b), the advantage of the modal transformation method is evident. The error, which shows as non-zero coefficients in the first and second higher order modes of both the symmetric and non-symmetric modes is lower for the modal transformation method. Only for the third highest radial order mode does the direct projection method enjoy a slight advantage, although the relative error at that high radial frequency in either case is low.

The overall effect is that the modal transformation method may be used to generate Zernike data inside the defined clear aperture region with less error than a competing strategy. The other significant conclusion is that to apply the modal transformation method, actuated regions must occur outside of the clear aperture region, thus increasing the complexity of the system. In this example, 39 per cent more actuators were required when using the modal transformation method, which would require an attendant amount of power and system integration. However, it is the opinion of the researchers that the performance gain, and the resulting decrease in the overall diameter of a mirror structure, would far outweigh the increase in complexity. A systems level trade study is foreseen as a potential future effort. Manufacture of a 61-actuator mirror is under construction with the assistance of the Material Science Division of the Air Force Research Laboratory which is projected to undergo testing in the spring of 2006.

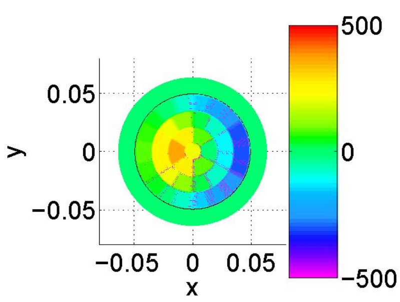

(a) Voltage distribution (in volts) on piezoelectric actuating grid for direct projection method.

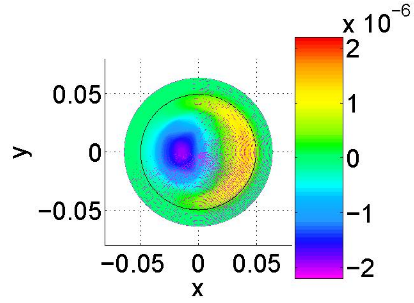

(b) FEM surface deflection for direct projection method.

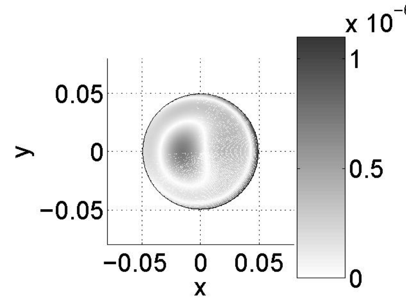

(c) Absolute error for direct projection method.

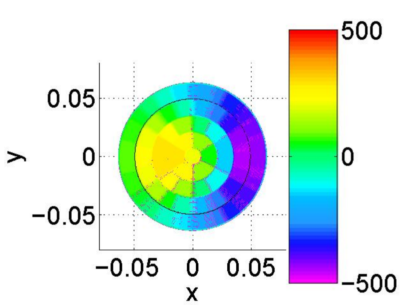

(d) Voltage distribution (in volts) for proposed modal transformation method.

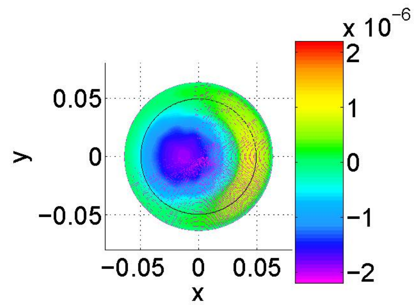

(e) FEM surface deflection for proposed modal transformation method.

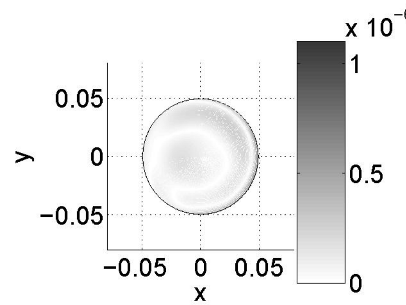

(f) Absolute error for proposed modal transformation method.

Fig. 11. Comparison of non-linear finite element model of proposed modal transformation method versus direct projection method for obtaining simultaneous defocus and tilt Zernike mode shapes across the clear aperture region. The clear aperture region is indicated by a black line at 0.78 of the surface radius. The error displayed is absolute error minus the Zernike piston mode error, which is the dominant error for both methods but of little consequence for optical reflectors. All dimensions are in meters unless otherwise indicated.

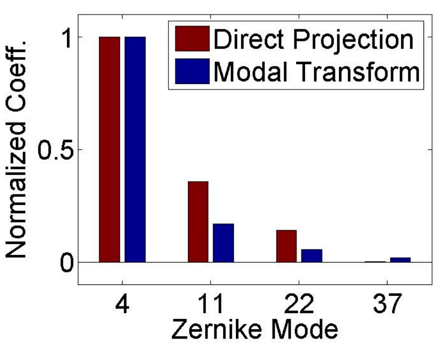

(a) Axisymmetric modes.

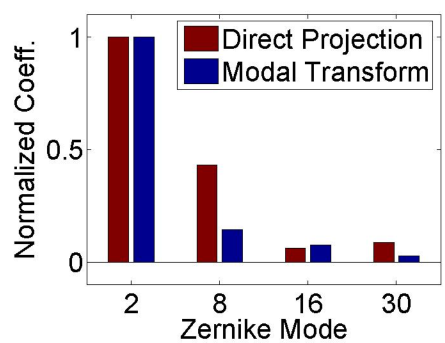

(b) Non-axisymmetric modes corresponding with $\cos\theta$ behavior.

Fig. 12. Comparison of Zernike mode coefficients for actuated surface for matrix modal transformation methodology versus direct projection methods as described in text. The desired Zernike modes were 2 and 4. Values of coefficients for other modes represent undesired surface deflection.

VI. Conclusions

The static shape control of a membrane mirror has been explored. Development of a methodology which prescribes the desired surface displacement of an interior, "clear aperture" region in terms of physically achievable mode shapes has been developed. In the development, surface error can be seen to be a function of the clear aperture radius relative to the mirror radius, and also as a function of the number and accuracy of achievable mode shapes, themselves a function of the fineness of the actuating grid.

In the example presented, a non-linear finite element model simulation of deformable circular mirror with 61-piezoelectric unimorph actuators showed the advantages of the proposed modal transformation method to determine actuator gains to create a desired surface when compared to a direct projection method based solely on solving the governing membrane equation.

Areas of further research as a direct result of questions posed in this paper include further efforts to accurately (and simply) model the structure to obtain the piezoelectric-actuated vibration mode shapes essential to the use of this method. Also, the need to invert the modal transformation matrix as presented in Section IV-D for higher order systems may require more advanced techniques. Finally, the unresolved scaling issues between represented Zernike modes observed in the finite element simulation are not fully understood and merit future study.

Despite these areas of research interest, the methods presented should be suitable for incorporation in the control of larger scale structures, and although presented for the continuous circular mirror, there is nothing in the method presented which prevents a similar strategy from being developed for annular or parabolic reflectors.

Greater complexity in the system due to the increase in number of actuators and the subsequent increased power requirement appears to be the main tradeoff for the increased accuracy in quasi-static surface deflection performance when applying this control methodology.

VII. Acknowledgements

The research presented in this document was conducted with the financial support of the Air Force Office of Scientific Research under the direction of Lieutenant Colonel Sharon Heise.

References

[1] Agnes, G. S. and Dooley, J., "Precision Deployable Structures Technology for NASA Large Aperture Missions," *Space 2004 Conference and Exhibit*, American Institute of Aeronautics and Astronautics, 2004.

[2] Acikmese, A., Mettler, E., Breckenridge, W. G., Macenka, S. A., and Tubbs, E. F., "L2 Earth Atmosphere Observatory: Formation Guidance, Metrology, and Control Synthesis," *AIAA/AAS Astrodynamics Specialist Conference and Exhibit*, American Institute of Aeronautics and Astronautics, Inc., 2004.

[3] Carreras, R. A., "On Near-Net Shape Membrane Optics," *AIAA Space Technology Conference and Exposition*, 1999.

[4] Ash, J. T., Jenkins, C. H., Marker, D. K., and Wilkes, J. M., "Shape Achievement of Optical Membrane MirrorsUsing Coating/Substrate Intrinsic Stresses," *Journal of Spacecraft and Rockets*, Vol. 41, No. 4, 2004, pp. 551–557.

[5] Vaughan, H., "Pressurising a Prestretched Membrane to form a Paraboloid," *J. Engng. Sci.*, Vol. 18, 1980, pp. 99–107.

[6] Jenkins, C. H., Wilkes, J. M., and Marker, D. K., "Improved Surface Accuracy of Precision Membrane Reflectors through Adaptive Rim Control," *39th AIAA/ASME/ASCE/AHS/ASC Structures, Structural Dynamics, and Materials Conference*, American Institute of Aeronautics and Astronautics, Inc., 1998.

[7] Wilkes, J. M., Jenkins, C. H., Marker, D. K., Carreras, R. A., Duneman, D. C., and Rotge, J. R., "Concave membrane mirrors from aspheric to near-parabolic," *High-Resolution Wavefront Control: Methods, Devices, and Applications*, edited by J. D. Gonglewski and M. A. Vorontsov, Vol. 3670, SPIE, 1999.

[8] Tokovinin, A., Thomas, S., and Vdovin, G., "Using 50-mm Electrostatic Membrane Deformable Mirror in Astronomical Adaptive Optics," *Advancements in Adaptive Optics*, edited by D. B. Calia, B. L. Ellerbroek, and R. Ragazzoni, Vol. 5490, SPIE, 2004, pp. 580–585.

[9] Flint, E. M. and Denoyer, K. K., "Approach for Efficiently Evaluating Internally Reacted Global Shape Control Actuation Strategies for Apertures," *44th AIAA/ASME/ASCE/AHS/ASC Structures, Structural Dynamics, and Materials Conference*, Vol. 2003, American Institute of Aeronautics and Astronautics, Inc., 2003.

[10] Pearson, J. and Hansen, S., "Experimental Studies of a Deformable-mirror Adaptive Optical System," *Journal Optical Society of America*, Vol. 67, No. 3, 1977, pp. 325–333.

[11] Noll, R. L., "Zernike Polynomials and Atmospheric Turbulence," *Journal Optical Society of America*, Vol. 66, No. 3, 1976, pp. 207–211.

[12] Meirovitch, L., *Principles and Techniques of Vibrations*, Prentice-Hall, Inc., 1997.

[13] Zwillinger, D., *CRC Standard Mathematical Tables and Formulae, 31st Edition*, CRC Press, 2003.

[14] Wagner, J. W., Agnes, G. S., and Magee, E., "Optical Metrology of Adaptive Membrane Mirrors," *Journal of Intelligent Material Systems and Structures*, Vol. 11, 2000, pp. 837–847.

[15] Sobers, D. M., Agnes, G. S., and Mollenhauer, D., "Smart Structures for Control of Optical Surfaces," *44th AIAA/ASME/ASCE/AHS/ASC Structures, Structural Dynamics, and Materials Conference*, American Institute of Aeronautics and Astronautics, Inc., 2003.

[16] Cote, F., Masson, P., Mrad, N., and Cotoni, V., "Dynamic and Static Modelling of Piezoelectric Composite Structures Using a Thermal Analogy With Msc/nastran," *Composite Structures*, Vol. 65, No. 3, 2004.

[17] Nayfeh, A. H. and Pai, P. F., *Linear and Nonlinear Structural Mechanics*, Wiley series in nonlinear science, Wiley-Interscience, 2004.

Michael Shepherd is a Ph. D. Candidate at the Air Force Institute of Technology. Maj Shepherd's research interests include structural dynamics of aerospace structures and flight test. Maj Shepherd obtained a B.S. in engineering mechanics from the USAF Academy in 1990, and a M.S. in aeronautical and astronautical engineering from the University of Washington in 1991. He is a graduate of the USAF Test Pilot School and a member of AIAA.

Richard Cobb is an Assistant Professor of Aerospace Engineering in the Department of Aeronautical and Astronautical Engineering, Air Force Institute of Technology, WPAFB, Ohio. His research focuses on dynamics and control of large structures for space-based remote sensing and structural health monitoring for aerospace applications. Dr. Cobb received his B.S. in aerospace engineering from the Pennsylvania State University in 1988, an M.S. in astronautical engineering from the Air Force Institute of Technology in 1992, and a Ph.D. from the Air Force Institute of Technology in 1996. Dr. Cobb is a member of SPIE and a senior member of AIAA.

William Baker William Baker is an Associate Professor of Applied Mathematics in the Department of Mathematics and Statistics, Air Force Institute of Technology, WPAFB Ohio. His research interest is in asymptotic analysis applied to nonlinear dynamics and in wave propagation theory. Dr. Baker received his BA and MA from the University of California at Irvine in 1970 and his PhD from Northwestern University in 1987.